ADAPTIVE OPTICS SPECTROSCOPY OF THE [Fe II] OUTFLOW FROM DG TAURI [1]

Tae-Soo Pyo, Naoto Kobayashi, Masahiko Hayashi, Hiroshi Terada, Miwa Goto, Hideki Takami, Naruhisa Takato, Wolfgang Gaessler, Tomonori Usuda, Takuya Yamashita

Subaru Telescope, National Astronomical Observatory of Japan, 650 North A'ohōkū Place, Hilo, HI 96720, USA

Alan T. Tokunaga

Institute for Astronomy, University of Hawaii, 2680 Woodlawn Drive, Honolulu, HI 96822, USA

Yutaka Hayano, Yukiko Kamata, Masanori Iye

National Astronomical Observatory of Japan, Mitaka, Tokyo 181-8588, Japan

and

Yosuke Minowa

Department of Astronomy, School of Science, University of Tokyo, Tokyo 113-0033, Japan

ABSTRACT

We present results of the velocity-resolved spectroscopy of the [Fe II] $\lambda 1.644$ μm emission line along the optical jet emanating from DG Tau. The slit spectrum, obtained with the Subaru Telescope Adaptive Optics System at an angular resolution of $0\farcs16$, shows strong, entirely blueshifted emission on the southwestern side of the star. A faint, redshifted counter feature was also detected on the northeast side with emission within $0\farcs7$ of the star being occulted by the circumstellar disk. The blueshifted emission has two distinct radial velocity components. The low-velocity component (LVC) has a peak radial velocity of ~ -100 km s^{-1} with an FWHM line width of $\sim$100 km s^{-1}, and it peaks at $0\farcs2$–$0\farcs5$ from the star. The high-velocity component (HVC) peaks at $0\farcs6$–$0\farcs8$ away from the star showing a peak radial velocity of ~ -220 km s^{-1} with a line width of $\sim$50 km s^{-1}. These characteristics are remarkably similar to the [Fe II] outflow from L1551 IRS 5, although the linear scales of the HVCs and LVCs are different for the two objects. We conclude, as an analogy to the case of L1551 IRS 5, that the HVC is a well-collimated jet launched from the region close to the star and the LVC is a disk wind with a wide opening angle. Detailed comparison of emission parameters between the two sources, however, suggests that part of the LVC emission from DG Tau arises from the gas entrained and accelerated by the HVC, if we assume continuous steady-state outflows. The presence of two distinct emission components clearly separated in space and velocity may favor theoretical models with two outflows: one is the LVC magnetohydrodynamically driven near the inner edge of an accretion disk, and the other is the HVC driven by the reconnection of dipolar stellar magnetic fields anchored to the disk.

Subject headings: ISM: Herbig-Haro objects — ISM: individual (DG Tau, HH 158) — ISM: jets and outflows — stars: formation — stars: pre-main sequence — techniques: high angular resolution

1. INTRODUCTION

High-velocity outflows from young stellar objects (YSOs) are closely related to the accretion process of star formation and may play important roles in removing angular momentum from a star-disk system. Studies of YSO outflows may provide us with crucial information for understanding the physical process of star formation. It has been reported that T Tauri stars often show collimated outflows within a few arcseconds of the driving sources. They are called "small-scale jets" (Eislöffel et al. 2000) or "micro jets" (Solf 1997; Hirth, Mundt, & Solf 1994a, 1997). Such small-scale outflows are the best targets for a study of the collimation and acceleration mechanisms of outflows and their relation to the accretion process because they are in the vicinity of the driving sources.

High-resolution optical spectroscopy revealed that many classical T Tauri stars exhibit forbidden emission lines with double-peaked profiles. The HVC has the radial velocity between -50 and -200 km s^{-1} with respect to the stellar velocity, while the LVC shows the radial velocity between -5 and -20 km s^{-1}. The two velocity components are different in their spatial distributions and kinematical and physical characteristics (Hamann 1994; Hirth et al. 1994b; Hirth, Mundt, & Solf 1994a, 1997; Hartigan, Edwards, & Ghandour 1995), which led Kwan & Tademaru (1988, 1995) to propose a model with two different outflows: the HVC is a jet emanating from the region close to the star, while the LVC is a wind

[1]Based on data collected at Subaru Telescope, which is operated by the National Astronomical Observatory of Japan.

originating from the accretion disk. The two outflows are, however, not independent from each other, as shown by the tight correlation in their luminosities (Calvet 1997). This fact suggests the possibility that both are closely related to the accretion activities of the star-disk system, such as the rate of mass inflow in the disk as well as that from the disk onto the star.

In a previous contribution, we presented a position-velocity diagram for the [Fe II] $\lambda 1.644$ μm emission from the L1551 IRS 5 outflow (Pyo et al. 2002) showing the presence of HVC and LVC well separated from each other in radial velocity and space. In fact, our results have revealed the following characteristics much more clearly than before: (1) There are two distinct velocity components that are blueshifted with respect to the stellar velocity. (2) The HVC and LVC are qualitatively different from each other as evidenced by the facts that the HVC consistently shows a narrow line width and is more extended and located farther away from the origin than the LVC, which has a broad line width. These results may support the two outflows model for young stellar outflows.

To extend our studies, we present new results of the [Fe II] $\lambda 1.644$ μm line observations toward DG Tau in this paper. DG Tau is an "extreme" T Tauri star showing a flat spectral energy distribution (SED) from near- to far-infrared wavelengths. The flat spectrum was explained by the thermal emission from a circumstellar disk (Adams, Emerson, & Fuller 1990) in combination with a flattened infalling envelope (Calvet et al. 1994). These observations suggest that DG Tau is in the transition phase from an embedded protostar to a revealed classical T Tauri star.

DG Tau has an associated optical jet called HH 158, which has been one of the best studied in optical forbidden lines. The jet extends up to $\sim 10''$ to the southwest from the star with the position angle of $\sim 225°$ (Mundt & Fried 1983). The inclination angle of the jet axis, with respect to the line of sight, is $\sim 32°$ estimated from the proper motion and radial velocity (Eislöffel & Mundt 1998). Observations of [O I] $\lambda 0.6300$ μm and [S II] $\lambda 0.6731$ μm lines showed that the jet has the HVC and LVC at ~ -250 km s^{-1} and ~ -50 km s^{-1}, respectively (Hartmann & Raymond 1989; Hamann 1994; Hartigan, Edwards, & Ghandour 1995). Solf & Böhm (1993) suggested from their long-slit spectroscopy at a resolution of ~ 10 km s^{-1} that the LVC is compact, while the HVC is extended within $\pm\ 4''$ from the star, although their spatial resolutions ($0\overset{''}{.}7$–$1\overset{''}{.}5$) were not sufficient to resolve a subarcsecond structure in detail.

It gradually became evident for DG Tau that the HVC is nested inside the LVC. From optical spectroscopy with a slit perpendicular to the jet, Mundt, Brugel, & Bührke (1987) found that the spatial width of the HVC (-240 km s^{-1}) is three times narrower than that of the LVC (-150 km s^{-1}), with the LVC showing a radial velocity 30–60 km s^{-1} slower at the edges than at the center. The narrower width of the HVC implies that it is spatially located inside the LVC and closer to the axis of the outflow. Spectro-imaging observations at a subarcsecond resolution have confirmed such a view, showing that the HVC is spatially narrow and well collimated around the axis of the jet, while the LVC is spatially wide (Lavalley et al. 1997; Lavalley-Fouquet, Cabrit, & Dougados 2000; Bacciotti et al. 2000).

In this article, we present new results of the [Fe II] $\lambda 1.644$ μm line spectroscopy toward the outflow from DG Tau that shows the strong emission of this line (Hamann et al. 1994). The [Fe II] line is one of the strongest forbidden transitions in the near-infrared, where the extinction is much smaller than that at visible wavelengths. In addition, the data was obtained with a high spatial resolution of $0''.16$ achieved with the Subaru Telescope Adaptive Optics System, thus allowing us to study the detailed spatial and radial velocity structure of the outflow within an arcsecond from the star.

2. OBSERVATIONS AND DATA REDUCTION

The observations of the DG Tau jet were made on 2001 October 31 as part of a commissioning run of the Infrared Camera and Spectrograph (IRCS; Kobayashi et al. 2000; Tokunaga et al. 1998) combined with the Adaptive Optics (AO) System, both mounted together at the Cassegrain focus of the Subaru Telescope atop Mauna Kea, Hawaii. Near-infrared spectra over the H-band were obtained with the IRCS echelle spectrograph equipped with a Raytheon 1024×1024 InSb array with an Aladdin II multiplexer. The pixel scale[2] was $0''.060 \pm 0''.006$ pixel^{-1}. Under poor seeing conditions exceeding $1''$, the AO system allowed us to reach the angular resolution of $0''.16$ (FWHM) in the H band. The slit width chosen was $0''.3$, and the resulting velocity resolution was 30 km s^{-1} ($\lambda/\Delta\lambda \sim$ 10,000). The slit length was $3''.8$. The spectrum was taken along the jet with a position angle (PA) of $\sim$222°, which was determined by the position angle of knot A in Eislöffel & Mundt (1998). The total on-source exposure time was 320 s. Sky frames were observed at $30''$ west of DG Tau. We observed the standard star HD 290798 (A2V, $T_{\rm eff}$ = 8810 K, V = 10.40 mag) for calibrating the flux and removing telluric absorption.

We reduced the data by using IRAF packages. We subtracted the dark current from each frame, flat-fielded the object frames with a normalized flat frame using the APNORMALIZE task, and corrected bad pixels and cosmic ray events. Each order of the spectra was extracted as a "spectral image" by using the APALL task with the "strip" option for

[2]The pixel scale of $0''.075$ pixel^{-1} given in Pyo et al. (2002) has turned out to be incorrect, although this does not alter the main conclusions of their paper.

the output format parameter. We then corrected the spectra for distortion of the slit images, performed the wavelength calibration, and subtracted the night sky, OH airglow emission lines, and stellar continuum with the tasks such as IDENTIFY, REIDENTIFY, FITCOORDS, TRANSFORM, and BACKGROUND in the *noao.twodspec.longslit* package. Wavelength sensitivity correction and flux calibration were performed with the spectra of the standard star and a blackbody that had the same $T_{\rm eff}$ and V magnitude as the standard star. Because the standard star showed a broad Br12 absorption line, we corrected it with the SPLOT task before using its spectrum to divide into the DG Tau spectra to remove the telluric absorption and instrumental throughput.

3. RESULTS

3.1. High and Low Velocity Components

Figure 1 shows a continuum-subtracted [Fe II] $\lambda 1.644$ μm emission spectrum along the DG Tau jet presented as a position-velocity diagram (PVD). The emission corresponding to the blueshifted outflow[3] is seen at $Y \gtrsim 0\farcs15$, where Y is the projected angular distance measured along the optical jet (P.A. = 222°) from the star. A faint, counter outflow emission is also seen on the redshifted side at $Y < -0\farcs7$. The stellar continuum level was determined at each velocity side of the [Fe II] emission, one at -1100 ± 100 km s^{-1} and the other at $+1100 \pm 100$ km s^{-1} with respect to the [Fe II] line rest velocity, linearly interpolated into inbetween velocities, and subtracted. The PVD at $|Y| \lesssim 0\farcs23$, where significant stellar continuum emission exists, is affected by the jagged, periodic positive and negative feature caused by the detector undersampling[4] and photospheric (K7–M0) and telluric absorption lines.

At the southwest of DG Tau ($Y > 0''$), the entire [Fe II] emission is blueshifted with respect to the systemic radial velocity of $V_{\rm LSR} = +6.4$ km s^{-1} (Kitamura, Kawabe, & Saito 1996), with no emission observed around the velocity. This suggests that the emission originates entirely from outflows, as was the case for the outflow from L1551 IRS 5 (Pyo et al. 2002). The blueshifted [Fe II] emission has two distinct radial velocity components with similar peak intensities: the LVC at $V_{\rm LSR} \sim -100$ km s^{-1} and the HVC at $V_{\rm LSR} \sim$

---

[3]We use the general word "outflow" when we do not know its morphology such as the opening angle. We use the word "jet" for a collimated outflow with a small opening angle and "wind" for a less collimated outflow with a large opening angle, although this choice is somewhat arbitrary.

[4]This effect is caused when a point spread function is not sufficiently sampled along the slit (spatial direction) and the spectrum is tilted on the array. See Freudling (1999) for details.

-220 km s^{-1}.

Figure 2 shows the line profiles of [Fe II] emission presented at every $0''.6$ interval for the blueshifted outflow. We applied multiple Gaussian fitting to these line profiles to obtain the spatial variations of the peak intensity, peak radial velocity, and velocity width for the HVC and LVC. We took into account the Br12 emission (λ1.6412 μm) for the Gaussian fitting at $Y \leq 0''.42$, where the emission line is strong. It occurs at $V_{\rm LSR} \sim -480$ km s^{-1} with respect to the [Fe II] line rest wavelength and has a FWHM width of 191 $\pm$ 14 km s^{-1}. It does not affect the [Fe II] emission at $|Y| \gtrsim 0''.23$, which we will discuss later in this paper. The spatial variations are shown in Figure 3, where the dotted parts of the lines represent the positions where the emission peaks for the HVC or LVC were not visually identified with confidence in Figure 2.

The line profiles of the LVC have discernible peaks at the positions with $0''.24 \leq Y \lesssim 0''.71$, while the peaks become unclear at $Y \gtrsim 0''.71$, where the LVC feature is seen as a wing to the HVC. A sharp peak is seen at $V_{\rm LSR} \sim -60$ km s^{-1} at $Y \lesssim 0''.24$. Although this might be a spurious feature caused by the periodic undersampling effect noted above, it may correspond to the knot A feature seen at a similar radial velocity in the [S II] λ6731 and [O I] λ6300 emissions in the vicinity of the star (Solf & Böhm 1993). The peak intensity of the LVC is strong at $0''.24 \leq Y \lesssim 0''.5$ and decreases with the distance from the driving source. The peak radial velocity changes from $V_{\rm LSR} = -60$ to -120 km s^{-1} as the position moves from $Y \lesssim 0''.24$ to $0''.71$. The peak radial velocity of the LVC continues to achieve higher negative values at $Y \gtrsim 0''.71$, where its peaks are not clearly identified. The FWHM width of the LVC increases from $\sim$50 km s^{-1} at $Y = 0''.24$ to $\sim$120 km s^{-1} at $0''.71$. It tends to be constant at $Y \gtrsim 0''.77$, although the "line width" is not well defined in this range, where the LVC appears to be a wing feature to the HVC.

The line profiles of the HVC show discernible peaks at $0''.5 \lesssim Y \lesssim 1''.3$. The peak intensity increases with distance at $Y \leq 0''.65$, is strongest around $Y = 0''.65$–$0''.85$, and decreases at $Y \gtrsim 0''.85$. A radial velocity variation is prominent in the HVC. Its peak radial velocity is $V_{\rm LSR} = -240$ km s^{-1} at $Y = 0''.5$, becomes less blueshifted to -210 km s^{-1} at $Y = 0''.9$, and then returns to -240 km s^{-1} at $Y = 1''.2$, showing a bow-shaped feature on the PVD. The peak radial velocity shows a hint to be less blueshifted toward the star at $Y \lesssim 0''.5$ and along the distance from the star at $Y \gtrsim 1''.3$, implying a sinusoidal variation. The FWHM line width of the HVC first decreases from 160 km s^{-1} at $Y = 0''.42$ to 70 km s^{-1} at $Y \sim 0''.65$, and then becomes constant at 50 km s^{-1} at $Y \gtrsim 0''.77$.

It should be noted that the radial velocity of the LVC of DG Tau is considerably larger than those of many other T Tauri outflows measured from optical forbidden lines. It might not be appropriate that we assume the LVC of DG Tau to have the same nature as those of the others. For example, the possibility of coronal disk emission is not ruled out for the LVC with a velocity of just a few km s^{-1}. In this sense the term LVC should not be considered to have any physical basis, but should be taken to describe relative radial velocities of outflows emanating from individual sources. In the case of DG Tau, the HVC and LVC of the [Fe II] emission have similar velocities to the HVC and LVC, respectively, of optical forbidden lines (see § 1).

3.2. Counter Outflow Emission

Another important feature in Figure 1 is the redshifted counter outflow. The counter emission suddenly appears at $Y = -0\farcs7$, suggesting that the inner part of the receding outflow is hidden behind an optically thick circumstellar disk. The projected disk radius agrees well with the minor axis radius of $0\farcs6$ of the 2.7 mm disk emission (Dutrey et al. 1996). Assuming 45° as the inclination of the outflow axis and the distance of 140 pc to DG Tau, we estimate the radius of the optically thick disk to be 140 AU.

The counter outflow emission ranges from $V_{\rm LSR} = 80$ to 240 km s^{-1} with a peak around 200 km s^{-1} at $Y \sim 0\farcs9$. The radial velocity range suggests that both HVC and LVC were detected in the receding outflow. The slanting pattern of the emission edge at the farther side seen in the PVD matches well with that of the corresponding approaching outflow, implying an intrinsically symmetric emission pattern with respect to the origin of the PVD. The intensity of the redshifted counter emission is 10 times weaker than the corresponding blueshifted emission at the same distance from DG Tau. Assuming that the redshifted counter emission intrinsically has the same intensity as the blueshifted one, we derive the extinction to the counter outflow at $Y \sim -1\farcs0$ to be ~2.5 mag at λ1.644 μm. This value corresponds to $A_{\rm V} \approx 14.2$ mag based on the reddening law of Mathis (2000).

4. DISCUSSION

4.1. Comparison with L1551 IRS 5

Considering the results given in the previous section, we note that there are remarkable similarities in the blueshifted [Fe II] emission between DG Tau and L1551 IRS 5 as summarized below.

1. Both objects show two distinct radial velocity components which are entirely blueshifted with respect to their systemic velocities, suggesting the outflow origin of the emis-

sion.

2. The LVCs have the radial velocity of ∼100 km s^{-1} and are characterized by a broad line width of 100–200 km s^{-1} (FWHM). The HVCs have the radial velocity of 200–300 km s^{-1} and show a narrower velocity width of ∼50 km s^{-1} (FWHM).

3. The HVCs are located farther away from the origin than the LVCs.

Such similarities between the two young stellar outflows allow us to assume that they share the same physical mechanisms of acceleration and collimation as well as the same outflow structure. We may thus apply the interpretation for the L1551 IRS 5 outflow to the case of DG Tau, concluding that the HVC is a spatially narrow, well-collimated jet, while the LVC is a disk wind with large opening angle. Although no counter outflow was detected for L1551 IRS 5, this is probably because of a larger extinction toward this prototypical embedded source.

The characteristics of the two outflows are, however, not completely the same in detail. We try to compare the two outflows quantitatively by applying the multiple Gaussian fitting method to the line profiles shown in Figure 3 of Pyo et al. (2002) for the L1551 IRS 5 outflow.[5] Figure 4 shows the spatial variations of the peak intensity, peak radial velocity, and velocity width of the HVC, LVC, and wing component for the outflow from L1551 IRS 5.

By comparing Figures 3 and 4, we see that the HVCs and LVCs for the two YSOs share the same characteristics noted above, especially if we assume that the weaker part of the LVC emission at $Y \gtrsim 0\farcs7$ for DG Tau corresponds to the red-wing component at $Y \gtrsim 1\farcs6$ for L1551 IRS 5. Although the peak position of the HVC intensity was not covered by the observations of Pyo et al. (2002), it is clear that the LVC peaks occur closer to the driving sources for the two outflows. The angular scales, i.e., actual linear scales, are different for the two outflows. However, this may not prevent us from further comparison because linear scales of outflows depend on their ages after ejection. Besides the linear scales, notable differences are summarized below:

1. The LVC of DG Tau achieves higher negative velocity as it moves away from the driving source, while that of L1551 IRS 5 exhibits little velocity variation.

2. The FWHM velocity width of the LVC increases with distance for DG Tau, while it decreases for L1551 IRS 5.

---

[5] Note that we used the correct pixel scale of $0\farcs060$ pixel^{-1} for the echelle spectrograph of IRCS.

The gradual trend of higher negative velocity with distance for the LVC of DG Tau (Fig. 3*b*) might imply that its nature is somewhat different from that of L1551 IRS 5 (Fig. 4*b*). However, the L1551 IRS 5 outflow does have a wing component that has a more blueshifted radial velocity than its LVC and shows a higher negative velocity with distance. Pyo et al. (2002) suggested that this tendency is understood if the wing component is the remnant LVC gas entrained and accelerated by the HVC. By analogy, we may explain the higher negative velocity with distance for the LVC of DG Tau if a significant part of its gas is entrained by the HVC.

We must be careful, however, because this argument is based on single slit observations with the assumption of continuous steady-state outflows, which may lead to incorrect conclusions if the outflow wiggles or has a series of bow shocks to produce the observed radial velocity variation. We also note that the outflow is observed where it emits the [Fe II] line and is heated by shocks, meaning that we did not see the entire structure and velocity field of the outflow. As for the wiggle of the DG Tau outflow, the jet images in Bacciotti et al. (2000) as well as Lavalley-Fouquet, Cabrit, & Dougados (2000) did not show any significant wiggle within $1''.5$ from the star, which may support our interpretation derived from the single slit observations. We will continue the discussion based on the continuous steady-state outflow assumption in § 4.1.

The increase in the LVC velocity width with distance in Figure 3*c* may also be understood in a similar context. Because the peak in the HVC around $Y = 0''.6$–$0''.8$ may be a bow shock, which produces a longitudinal velocity field to develop a broad wing emission (Hartmann & Raymond 1984; De Young 1986), the LVC velocity width should increase toward the bow shock if a significant part of the LVC gas is entrained in the shock front. The LVC velocity width stays almost constant at 150 km s^{-1} for $Y \gtrsim 0''.8$.

We interpreted the decrease in the LVC line width with distance seen in L1551 IRS 5 in terms of collimation under the assumption that the line width is determined by the outermost diverging streamlines of a continuous steady-state outflow. If we apply the same assumption to the increase of the LVC line width for DG Tau, the increase would mean that the low-velocity wind diverges more when it goes farther away from its origin. This interpretation seems rather unnatural considering that most of the outflows are more or less collimated. Thus we do not think that the increase in the LVC line width observed for DG Tau is explained by more diverging streamlines with distance. It should rather be interpreted as a result of entrainment as discussed above.

We would like to note that the HVCs for both DG Tau and L1551 IRS 5 show a decrease in their line widths near the origin. This might be the collimation of the HVCs if we make the same assumption as we did for the LVC of L1551 IRS 5. The *HST* image shows, however, no evidence that the HVC is collimated around $0\farcs4$–$0\farcs6$ away from the star (Bacciotti et al. 2000), and it is too early for us to conclude that the narrowing of the HVC line width with distance manifests the collimation of the HVC gas.

4.2. Two Driving Mechanisms

There are two types of interpretation for the high- and low-velocity components of forbidden emission lines from young stars. One type argues that the two components are the inner and outer parts of a single outflow: the better-collimated, inner part appears as the HVC, whereas the less collimated, outer part is observed as the LVC (e.g., Edwards et al. 1987; Hartmann & Raymond 1989; Gómez de Castro & Pudritz 1993; Ouyed & Pudritz 1993, 1994; Bacciotti et al. 2000). The other type suggests that the two components correspond to two different outflows, such that the LVC is a poorly collimated disk wind, while the HVC is a jet launched separately from the region closer to the star (e.g., Kwan & Tademaru 1988, 1995). In this context, it is important that both DG Tau and L1551 IRS 5 show two "distinct" radial velocity components unambiguously separated from each other as the HVC and LVC on the PVDs. If observations did not clearly separate the two components in space and velocity but just showed that the two had different characteristics, they might have naturally led to the interpretation which favors a single outflow with its physical condition gradually changing from inside to outside. Our results hence give reasonable support to the two different outflow interpretations.

The presence of two distinct outflows suggests two different driving mechanisms of young stellar outflows, i.e., magnetohydrodynamically driven disk winds and reconnection driven stellar jets. The disk winds are driven by the interaction of an accretion disk with frozen-in magnetic fields and are centrifugally accelerated (e.g., Shu et al. 1994a,b, 1995; Königl 1989; Pudritz & Norman 1983, 1986; Kudoh & Shibata 1995, 1997a), with magnetic pressure acceleration being effective under certain conditions (Uchida & Shibata 1985; Shibata & Uchida 1986; Kudoh & Shibata 1997b). The reconnection driven winds are, on the other hand, produced when dipolar stellar magnetic fields anchored to the inner part of an accretion disk twist around due to the differential rotation between the star and the disk and periodically reconnect to release the magnetic energy as hot plasma observed as X-ray flares (Hayashi, Shibata, & Matsumoto 1996; Hirose et al. 1997; Goodson, Winglee, & Böhm 1997; Goodson, Böhm, & Winglee 1999; Goodson & Winglee 1999). Because the simulations of reconnection driven winds naturally include the disk winds (Hayashi, Shibata, & Matsumoto 1996; Hirose et al. 1997; Goodson, Böhm, & Winglee 1999), we expect that both driving mechanisms work simultaneously in the vicinity of accreting stars, producing two types of outflows as observed in DG Tau and L1551 IRS 5. Because both driving mechanisms are closely related to the accretion from the innermost part of a disk onto a star, there is no wonder that the luminosities of the HVC and LVC are tightly correlated (Calvet 1997) even if they are driven by the different mechanisms.

4.3. Proper Motions of Knots

We investigated the time variation of knot positions located within 5″ from DG Tau in order to examine their proper motions. Because of frequent observations of DG Tau in the last decades, it is not very difficult to interrelate the knot positions as shown in Table 1 and Figure 5. Although we must be careful that the identification of knots observed at different epochs is not unique, we believe that our identification is correct because most of the knot positions consistently lie along the straight lines in Figure 5.

The most conspicuous knot, B1, at $Y = 2\farcs6$ in 1994 November (Lavalley et al. 1997) corresponds to the one located at $Y = 3\farcs3$ in 1997 January, as was pointed out by Dougados et al. (2000), and to the one at $Y = 3\farcs6$ in Lavalley-Fouquet, Cabrit, & Dougados (2000). These three epochs of observations give the proper motion of $0\farcs272$ yr^{-1} for this knot, suggesting that the knot located at $Y = 2\farcs2$ in Solf & Böhm (1993) was the same one. The proper motion implies the epoch of ejection in 1985 for this knot.

Kepner, Hartigan, & Yang (1993) pointed out that the knot (KHY1) located at $0\farcs25$ away from DG Tau might coincide with the feature C of Solf & Böhm (1993). It may correspond to the feature called a low-velocity extension located at $1\farcs4$ (Lavalley et al. 1997), if we assume its proper motion to be similar to that of B1. Solf (1997) showed that the feature C became faint from 1992 to 1994, and this knot has not been identified thereafter.

Another conspicuous knot was detected in the [O I] emission by Dougados et al. (2000) at $Y = 0\farcs6$ in 1997 January and at $0\farcs9$ in 1997 December (also seen in Lavalley-Fouquet, Cabrit, & Dougados 2000). It was clear from Figure 5 that this knot corresponds to the bow shock A1 located at $1\farcs3$ in 1999 January (Bacciotti et al. 2000) and the knot at $0\farcs1$ in 1994 November (Lavalley et al. 1997). The proper motion estimated from these observations is $0\farcs275$ yr^{-1}, the same as that of B1.

Bacciotti et al. (2000) pointed out another well-defined structure, A2, at $Y = 0\farcs7$ on their slit scan images. Although its position is close to the HVC peak in our observations, we do not believe that our HVC peak corresponds to A2 because the “typical” proper motion derived above would locate A2 at $Y \sim 1\farcs5$ at the time of our observations. Instead, our

HVC peak shows better correspondence to the HVC peak detected by Takami et al. (2002) in their [Fe II] $\lambda 1.257\mu$m spectrum. Their PVD shows the HVC and LVC at $\sim 0\farcs3$ and $0\farcs16$, respectively, along the north-south slit. When we convert these values to the ones along the jet position angle, the HVC and LVC were located at $\sim 0\farcs45$ and $0\farcs23$, respectively, along the DG Tau outflow in 2000 December. These positions give the proper motions of $0\farcs34$ yr^{-1} and $0\farcs28$ yr^{-1} for the HVC and LVC, respectively, which are consistent with the "typical" proper motion for the other knots. The ejection epochs for the HVC and LVC are between late 1999 and early 2000; these are the latest ejection events so far. Figure 5 implies that knots were ejected every 5 years in the last two decades.

The proper motion for the HVC corresponds to the tangential velocity of 225 km s^{-1}, which is similar to its radial velocity, suggesting that it was ejected at an inclination angle of $\sim 45°$ with the actual velocity of ~ 300 km s^{-1}. The proper motion for the LVC corresponds to the tangential velocity of 185 km s^{-1} and is significantly larger than its radial velocity of ~ 100 km s^{-1}. The larger tangential velocity may imply that the LVC knot might be part of the shocked gas entrained and accelerated by the HVC.

5. SUMMARY

We observed the optical jet from DG Tau in the [Fe II] $\lambda 1.644$ μm emission line using the Subaru Telescope Adaptive Optics System. With the high angular and spectral resolutions, $0\farcs16$ and 30 km s^{-1}, respectively, the radial velocity structure of the [Fe II] outflow has been revealed within $\pm$ $1\farcs6$ from the star. The main results are summarized as follows:

1. The blueshifted [Fe II] emission at the southwest of DG Tau shows two distinct radial velocity components clearly separated from each other in both space and radial velocity. The LVC is ~ 100 km s^{-1} blueshifted with respect to the stellar velocity and shows strong emission at $0\farcs2$–$0\farcs5$ from the star. It has a broad line width of ~ 100 km s^{-1}. The HVC has a radial velocity of ~ -220 km s^{-1} and is strong at $0\farcs6$–$0\farcs8$ from the star. Its velocity width is ~ 50 km s^{-1}. The entire emission range for the two components is blueshifted with respect to the stellar velocity.

2. The observed results are remarkably similar to the [Fe II] outflow from L1551 IRS 5, in the sense that both objects have two distinct radial velocity components with the entire emission range being blueshifted, the HVCs show narrower line widths than the LVCs, and the HVCs have peaks located farther away from the driving sources than the LVCs. This has led us to conclude that the HVC is a well-collimated jet emanating

from the region close to the star, while the LVC is a disk wind with a large opening angle.

3. Quantitative comparison of the emission line parameters of the [Fe II] outflows between DG Tau and L1551 IRS 5 revealed that the LVC from DG Tau shows a higher blueshifted peak radial velocity and larger FWHM velocity width with distance from the star. These tendencies are different from those of the LVC from L1551 IRS 5. This may be because part of the LVC emission from DG Tau arises from the gas entrained and accelerated by the HVC.

4. The presence of two distinct outflow components in both DG Tau and L1551 IRS 5 may imply that they represent two different driving mechanisms working simultaneously in the vicinity of the accreting stars: the reconnection of dipolar stellar magnetic fields anchored to an accretion disk drives the HVC, whereas the interaction of the inner part of the disk with open magnetic fields drives the LVC.

5. We investigated the proper motions of the knots in the optical jet within 5″ from DG Tau. The typical proper motion is $\sim$0″.28, corresponding to a projected velocity of $\sim$180 km s^{-1}, and is similar among the identified 5 ejection events, which seemed to occur with a period of rough 5 years.

6. A redshifted counter outflow feature was also detected. A 0″.7 gap of emission between the feature and the star suggests the presence of an optically thick circumstellar disk of 140 AU in radius. We derived a visual extinction of $A_{\rm V} \approx 14.2$ mag toward the counter outflow at 1″ northeast of DG Tau from the intensity ratio between the redshifted and blueshifted emissions.

We are grateful to the entire staff of the Subaru Telescope for their dedicated support of the telescope and observatory operations.

REFERENCES

Adams, F. C., Emerson, J. P., & Fuller, G. A. 1990, ApJ, 357, 606

Bacciotti, F., Mundt, R., Ray, T. P., Eislöffel, J., Solf, J., & Camezind, M. 2000, ApJ, 537, L49

Calvet, N. 1997, in IAU Symp. 182, Herbig-Haro Flows and the Birth of Low Mass Stars, ed. B. Reipurth & C. Bertout (Dordrecht: Kluwer), 417

Calvet, N., Hartmann, L., Kenyon, S. J., & Whitney, B. A. 1994, ApJ, 434, 330

De Young, D. S. 1986, ApJ, 307, 62

Dougados, C., Cabrit, S., Lavalley, C., & Ménard, F. 2000, A&A, 357, L61

Dutrey, A., Guilloteau, S., Duvert, G., Prato, L., Simon, M., Schuster, K., & Menard, F. 1996, A&A, 309, 493

Edwards, S., Cabrit, S., Strom, S. E., Heyer, I., & Strom, K. M. 1987, ApJ, 321, 473

Eislöffel, J., & Mundt, R. 1998, AJ, 115, 1554

Eislöffel, J., Mundt, R., Ray, T. P., & Rodrìguez, L. F. 2000, in Protostars and Planets IV ed. V. Mannings, A. P. Boss, & S. S. Russell (Tucson: University of Arizona Press), 815

Freudling, W. 1999, Algorithms for Extracting Spectra from NICMOS Grism Images (User Manual V 3.1) (ST-ECF)

Gómez de Castro, A., & Pudritz, R. 1993, ApJ, 409,748

Goodson, A. P., Böhm, K. H., & Winglee, R. M. 1999, ApJ, 524, 142

Goodwon, A. P., & Winglee, R. M. 1999, ApJ, 524, 159

Goodson, A. P., Winglee, R. M., & Böhm, K. H. 1997, ApJ, 489, 390

Hamann, F. 1994, ApJS, 93, 485

Hamann, F., Simon, M., Carr, J. S., & Prato, L. 1994, ApJ, 436, 292

Hartigan, P., Edwards, S., & Ghandour, L. 1995, ApJ, 452, 736

Hartmann, L., & Raymond, J. C., 1984, ApJ, 276, 560

Hartmann, L., & Raymond, J. C. 1989, ApJ, 337, 903

Hayashi, M. R., Shibata, K., & Matsumoto, R. 1996, ApJ, 468, L37

Hirose, S., Uchida, Y., Shibata, K., & Matsumoto, R. 1997, PASJ, 49, 193

Hirth, G. A., Mundt, R., & Solf, J. 1994, A&A, 285, 929

Hirth, G. A., Mundt, R., & Solf, J. 1997, A&AS, 126, 437

Hirth, G. A., Mundt, R., Solf, J., & Ray, T. P. 1994, ApJ, 427, L99

Kepner, J., Hartigan, P., Yang, C., & Strom, S. 1993, ApJ, 415, L119

Kitamura, Y., Kawabe, R., & Saito, M. 1996, ApJ, 457, 277

Kobayashi, N., et al. 2000, Proc. SPIE, 4008, 1056

Königl, A. 1989, ApJ, 342, 208

Kudoh, T., & Shibata, K. 1995, ApJ, 452, L41

Kudoh, T., & Shibata, K. 1997a, ApJ, 474, 362

Kudoh, T., & Shibata, K. 1997b, ApJ, 476, 632

Kwan, J., & Tademaru, E. 1988, ApJ, 332, L41

Kwan, J., & Tademaru, E. 1995, ApJ, 508, 186

Lavalley, C., Cabrit, S., Dougados, C., Ferruit, P., & Bacon, R. 1997, A&A, 327, 671

Lavalley-Fouquet, C., Cabrit, S., & Dougados, C. 2000, A&A, 356, L41

Mathis, J. S. 2000, in Allen's Astrophysical Quantities, ed. A. N. Cox (4th ed.; New York: Springer), 523

Mundt, R., Brugel, E. W., & Bührke, T. 1987, ApJ, 319, 275

Mundt, R., & Fried, J. W. 1983, ApJ, 274, L83

Ouyed, R., & Pudritz, R. E. 1993, ApJ, 418, 255

Ouyed, R., & Pudritz, R. E. 1994, ApJ, 423, 753

Pudritz, R. E., & Norman, C. A. 1983, ApJ, 274, 677

Pudritz, R. E., & Norman, C. A. 1986, ApJ, 301, 571

Pyo, T. -S., Hayashi, M., Kobayashi, N., Terada, H., Goto, M., Yamashita, T., Tokunaga, A. T., & Itoh, Y. 2002, ApJ, 570, 724

Shibata, K., & Uchida, Y. 1986, PASJ, 38, 631

Shu, F. H., Najita, J., Ostriker, E., & Shang, H. 1995, ApJ, 455, L155

Shu, F. H., Najita, J., Ostriker, E., Wilken, F., Ruden, S., & Lizano, S., 1994a, ApJ, 429, 781

Shu, F. H., Najita, J., Ruden, S., & Lizano, S., 1994b, ApJ, 429, 797

Solf, J. 1997, in IAU Symp. 182, Herbig-Haro Flows and the Birth of Low Mass Stars, ed. B. Reipurth & C. Bertout (Dordrecht: Kluwer), 64

Solf, J., & Böhm, K. H. 1993, ApJ, 410, L31

Takami, M., Chrysostomou, A., Bailey, J., Gledhill, T. M., Tamura, M., & Terada, H. 2002, ApJ, 568, L53

Tokunaga, A. T., et al. 1998, Proc. SPIE, 3354, 512

Uchida, Y., & Shibata, K. 1985, PASJ, 37, 515

This preprint was prepared with the AAS LaTeX macros v5.0.

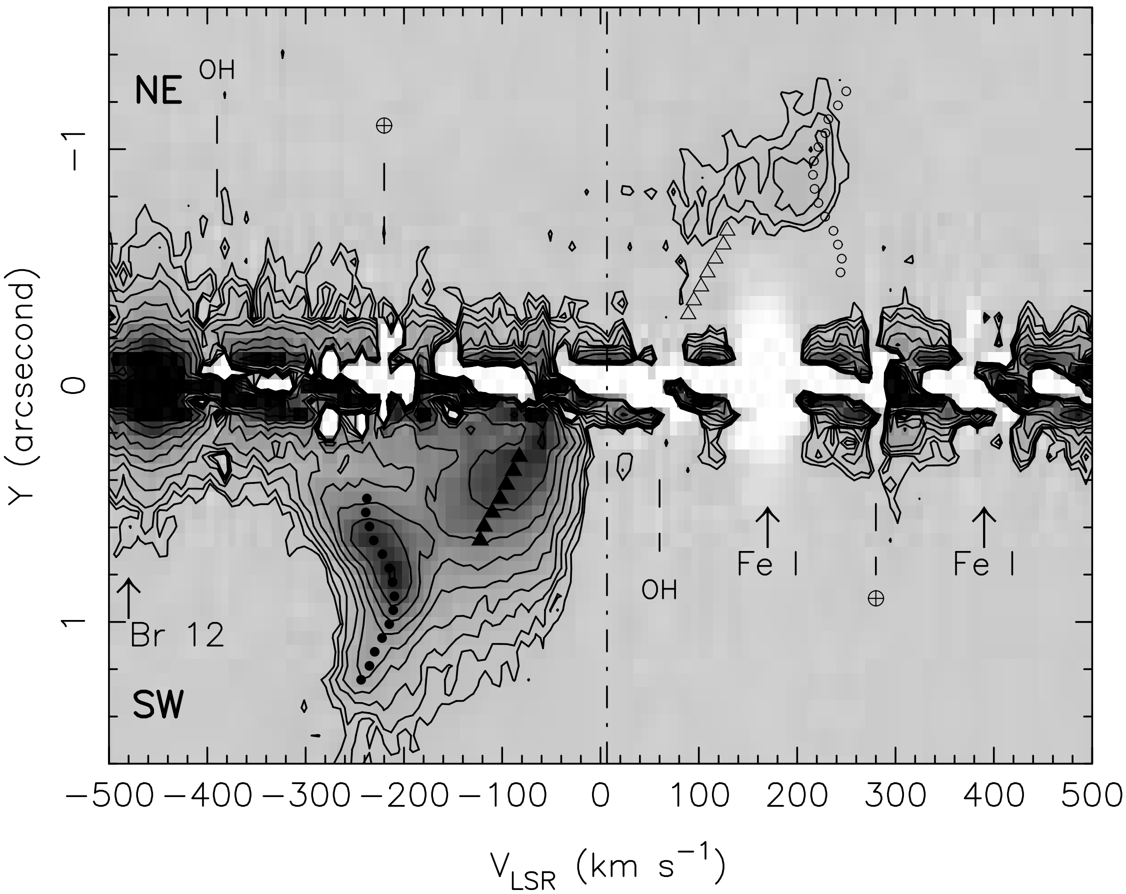

Fig. 1.— Continuum-subtracted position-velocity diagram of the [Fe II] λ1.644 μm emission along the optical jet from DG Tau (position angle = 222°). The region with positive Y corresponds to the southwest of DG Tau. Contours are drawn from 0.02×10^{-18} to 0.25×10^{-18} W m^{-2} Å^{-1} with equal intervals in a logarithmic scale. The jagged remnant of the stellar continuum is caused by the photospheric and telluric ($\oplus$) absorption lines and the Br12 emission line ($\lambda_{\rm vac}$ 1.6412 μm), and is affected by the undersampling of the detector. The dash-dotted vertical line shows the systemic velocity at $V_{\rm LSR} = +6.4$ km s^{-1} (Kitamura, Kawabe, & Saito 1996). Filled circles and triangles trace the peak velocities of the HVC and LVC, respectively. Open circles and triangles are the expected peak velocities for the counter outflows drawn symmetric to the filled ones with respect to the point at $Y = 0$ and $V_{\rm LSR} = +6.4$ km s^{-1}.

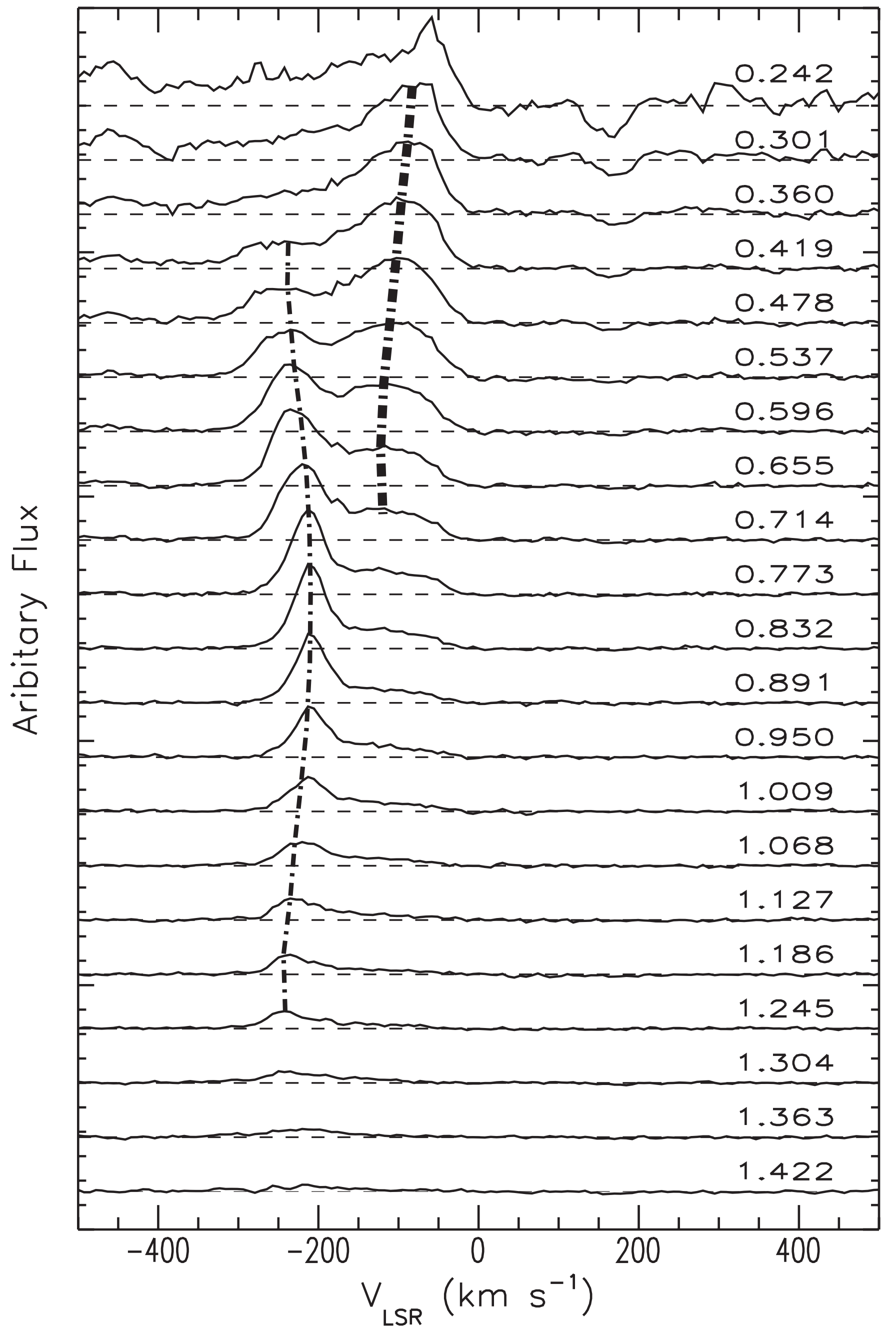

Fig. 2.— Line profiles of the blueshifted [Fe II] λ 1.644 μm emission lines extracted from Figure 1. Thin and thick dash-dotted lines show the peak velocities of the HVC and LVC, respectively. The column of numbers along the right side of each line profile shows the distance from the DG Tau in arcseconds.

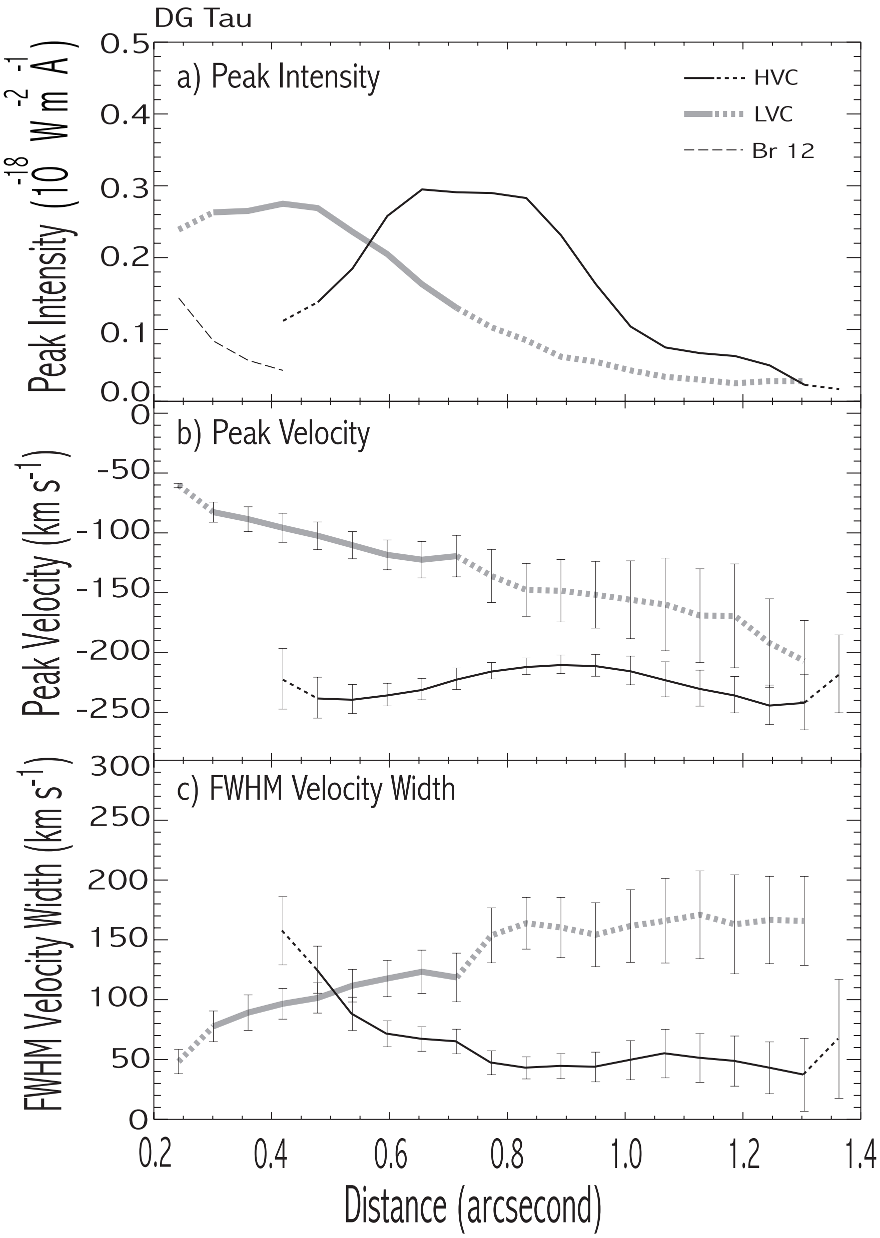

Fig. 3.— Variation of the peak intensity (a), peak radial velocity (b), and FWHM velocity width (c) of the [Fe II] emission with the distance from DG Tau. The thin solid and thick gray lines represent the high- and low-velocity components, respectively, with their dotted parts indicating the regions not visually identified with confidence on Figures 1 and 2. The thin dashed line is for the Br12 emission line.

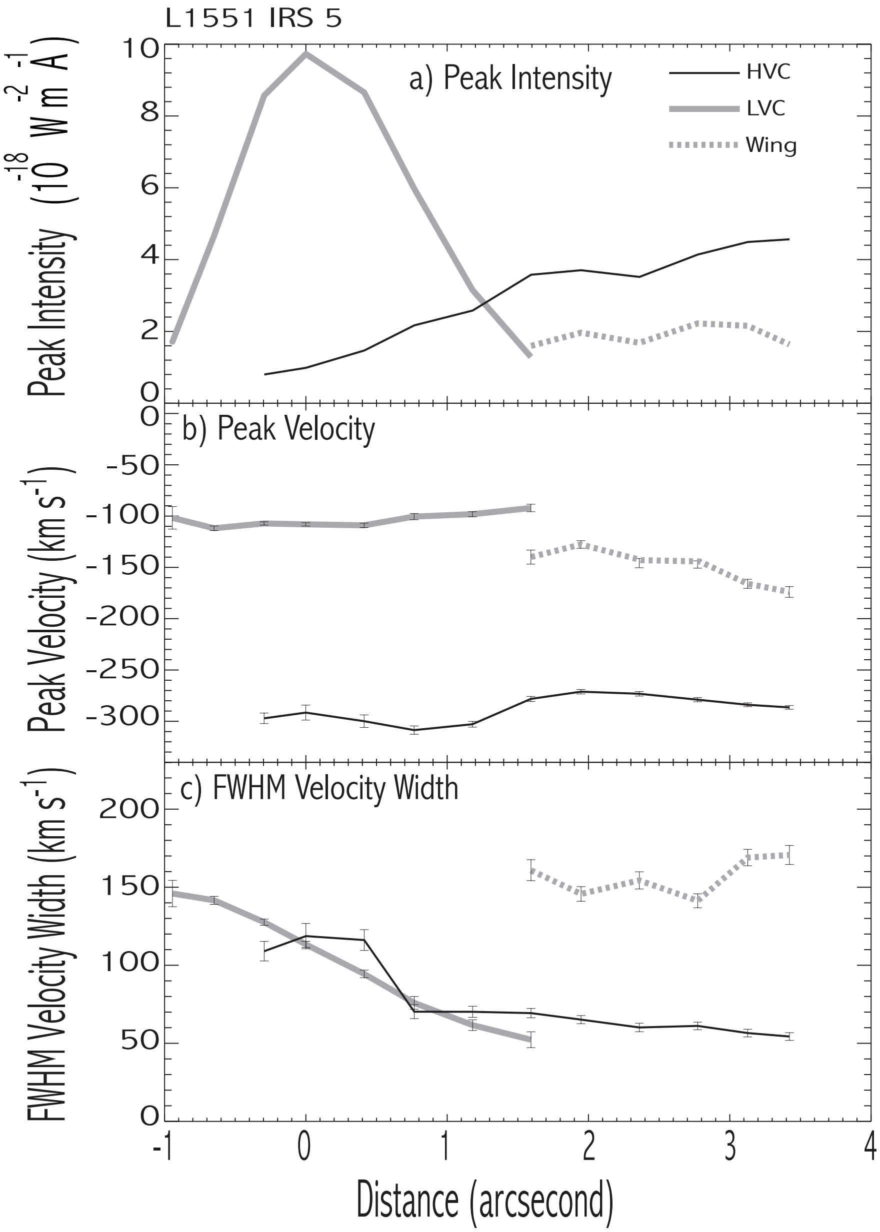

Fig. 4.— Same as Fig. 3, but for the [Fe II] outflows from L1551 IRS 5. The horizontal axis shows the distance from the peak (PHK1) of the low-velocity component. The L1551 IRS 5 VLA sources are located at $-1\farcs2$. The thin solid, thick gray, and thick dotted gray lines represent the high-velocity, low-velocity, and wing components, respectively. Note that the velocity width shows the values not deconvolved by the instrumental profile with the 59 km s^{-1} width (FWHM), which is twice that of the DG Tau observations. The FWHM width of 70 km s^{-1} corresponds to the deconvolved FWHM width of 40 km s^{-1}.

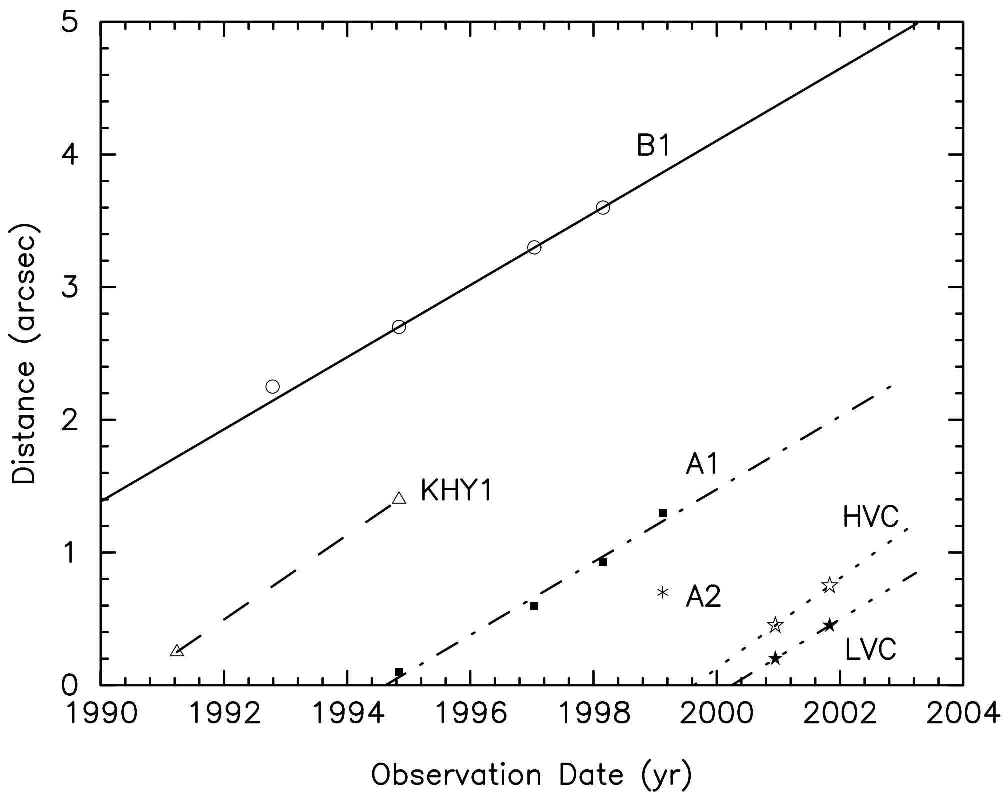

Fig. 5.— Time variation of knot positions along the optical jet of DG Tau in the last decade: knot B1 (open circles with a solid line), knot KHY1 (open triangles with a dashed line), knot A1 (filled squares with a dash-dotted line), knot A2 (an asterisk), HVC (open stars with a dotted line), and LVC (filled stars with a dash-triple-dotted line). See Table 1 for references.

Table 1. Knot positions and their proper motions within 5″ from DG Tau

Obs. Time	Distance (arcsec)						Ref.
	B1[a]	KHY1[b]	A1[c]	A2[c]	HVC	LVC	
1991 Mar. 27	···	0.25	···	···	···	···	1
1992 Oct.	2.25	···	···	···	···	···	2
1994 Nov. 3	2.7	*1.4*[d]	0.1	···	···	···	3
1997 Jan.	3.3	···	0.6	···	···	···	4
1998 Jan. 23-26	3.6	···	0.93	···	···	···	5
1999 Jan. 14	···	···	1.3	0.7	···	···	6
2000 Dec. 13	···	···	···	···	0.45	0.23	7
2001 Oct. 31	···	···	···	···	0.75	0.45	8
Proper motion	0.272 ± 0.001	0.3[e]	0.275 ± 0.024	···	0.34	0.28	···
Ejection Date	1985	1991	1994	···	1999–2000		···

[a]knot name taken from Lavalley et al. (1997).

[b]Kepner, Hartigan, & Yang (1993)

[c]knot name taken from Bacciotti et al. (2000).

[d]This is not an independent knot but an extension feature seen in Lavalley et al. (1997).

[e]Assumed value.

References. — (1) Kepner, Hartigan, & Yang (1993); (2) Solf & Böhm (1993); (3) Lavalley et al. (1997); (4) Dougados et al. (2000); (5) Lavalley-Fouquet, Cabrit, & Dougados (2000); (6) Bacciotti et al. (2000); (7) Takami et al. (2002); (8) This work